Shap. Mem. Superelasticity (2016) 2:196–203
DOI 10.1007/s40830-016-0066-z

SPECIAL ISSUE: RESEARCH ON BIOMEDICAL SHAPE MEMORY ALLOYS, INVITED PAPER

Radiopaque Shape Memory Alloys: NiTi–Er with Stable Superelasticity

Ausonio Tuissi[1] · Shane Carr[2] · James Butler[2] · Abbasi A. Gandhi[2] · Lisa O'Donoghue[3] · Karrina McNamara[2] · James M. Carlson[4] · Shay Lavelle[5] · Peter Tiernan[3] · Carlo A. Biffi[1] · Paola Bassani[1] · Syed A. M. Tofail[2]

Published online: 29 March 2016

Abstract Binary NiTi alloy is one of the most important biomaterials currently used in minimally invasive procedures and indwelling devices. The poor visibility of intermetallic NiTi under X-ray could be an unsatisfactory feature especially for developing low-dimensional implantable devices for the body. It is a matter of fact that the alloying of a third radiopaque element, such as noble or heavy metals, in NiTi can significantly enhance the alloy's radiopacity. Recently, it was demonstrated that the addition of a rare earth element such as Erbium has led to an equivalent radiopacity at a much lower cost than the equivalent addition of noble metals. This work reviews the main physical aspects related to the radiopacity of NiTi alloys and compares the radiopacity of NiTi–Er compositions with other NiTi-based alloys containing Pd, Pt, W and Cr. Furthermore, a NiTi–6Er alloy is produced by spark plasma sintering, and successfully processed by conventional hot and cold working procedures to a continuous wire showing stable superelastic behaviour (up to 4 % in strain), suitable for developing biomedical devices.

Keywords SMA · NiTi radiopacity · SMA processing · NiTiEr

Introduction

High X-ray visibility of surgical devices is critical to determine, during minimally invasive surgery, the exact placement of these devices within the targeted anatomical site, while keeping the X-ray exposure to the patient to a minimum [1, 2]. NiTi and common metallic biomaterials (e.g. stainless steel and Co–Cr alloys) used in minimally invasive surgery are inherently less visible due to their weak X-ray absorption ability (radiopacity) [1, 3]. Dense and high atomic number elements such as platinum (Pt) have been added to NiTi [1, 4–6] and stainless steel [7] to enhance radiopacity.

Adding one of the elements from the rare earth (RE) lanthanides can significantly enhance radiopacity [3, 8–10]. Lanthanides thus offer a much cheaper alternative to the addition of Pt. Except for cerium (Ce) [11–13], NiTi-RE system has practically received very little attention from a metallurgical point of view [14–16] perhaps due to the difficulty in subsequent processing of such alloys. The retention of the shape memory effect (SME) and superelasticity (SE) in NiTi-RE to a functional level is another challenge. Here we take NiTi–Er as a case study and show that this alloy can be conveniently prepared by spark plasma sintering (SPS) and subsequently processed by conventional hot and cold working to a wire which forms a suitable superelastic material for biomedical applications.

✉ Ausonio Tuissi
ausonio.tuissi@cnr.it

✉ Syed A. M. Tofail
Tofail.Syed@ul.ie

[1] Italian National Research Council, CNR- IENI Lecco Unit, Lecco, Italy

[2] Department of Physics and Energy, and Materials and Surface Science Institute, University of Limerick, Limerick, Ireland

[3] Department of Design and Manufacturing Technology, and Materials and Surface Science Institute, University of Limerick, Limerick, Ireland

[4] Med Institute, West Lafayette, IN, USA

[5] COOK Medical, Limerick, Ireland

Approach to Radiopacity Enhancement

Radiopacity generally refers to a material's capacity of X-ray absorption, which contrasts it against its surroundings in an X-ray image [2]. Like any other photon absorption, radiopacity is primarily governed by the Beer–Lambert Law which states that the amount of a photons transmitted through a material is dependent on its thickness and a material constant, linear attenuation coefficient, μ. If the size of the material decreases, the absorption decreases exponentially. In modern fluoroscopic X-ray imaging, a number of strategies are utilised to make part of the tissue or a material inside the body visible. Also, radiologists often use radiographic contrast agents to enhance visibility. Radiopacity of a material is thus fundamentally dependent on its absorption coefficient, which gives rise to the so called radiographic contrast.

We have found that certain rare earth (RE) elements in the lanthanide group can significantly improve radiopacity under clinically relevant X-ray imaging conditions [3, 9, 10]. The earliest reference to the addition of a rare earth element dates back to 1965 when Goldstein, Buehler and Wiley unsuccessfully attempted to add cerium (Ce) into NiTi [11]. Ce-added NiTi weld fillers have been investigated [12, 13]. Isothermal sections of experimentally derived ternary phase diagrams have also been reported showing apparently identical types of pseudo-binary phases of Ni–Dy, Ni–La and Ni–Nd in equilibrium with Ni–Ti phases [14–16]. The radiopacity of these alloys has not been discussed. Also, the feasibility of processing these alloys into a useful semi finished products was not reported.

Subject contrasts in X-ray radiography depend on material thickness, physical density, electron density, elemental composition and X-ray photon energy [17, 18]. For a given thickness of an object, the subject contrast is directly proportional to the difference ($\Delta\mu$) between the linear attenuation coefficients (μ) of the object and the background [2, 18]. The use of dense and higher atomic number (Z) elements (typically $Z = 72$–79 e.g. Pt, Au, Ta, W) improves radiopacity by increasing the linear attenuation coefficient in accordance with the power law $\mu = \frac{AZ^3}{E^3}$, where A is a proportionality constant and E is the energy of the photon. So, for a given element, μ falls off rapidly with the energy of the photon. Lower energy photons are thus absorbed more and higher energy photons absorbed less.

However, there are discontinuities in this falling off due to electronic transitions at X-ray absorption edges, which are characteristic of the electronic distribution of the elemental constitution of the object. At the X-ray absorption, edge quanta of energies are absorbed and μ jumps up to reach some discrete values and then falls off again as the photon energy increases in accordance with the power law until another electronic transition takes place.

The K-absorption edge lies between 39 and 64 keV for lanthanides and between 65 and 81 keV for elements with Z between 72 (Hf) and 79 (Au). Typical peak values of the white X-ray photon spectra used for common medical X-ray imaging, except for mammography, lie between 30 and 50 keV when X-ray is generated with a tube voltage between 40 and 120 kVp, respectively [18]. The attenuation of the imaging photon spectra by different filters, the air kernel between the X-ray source and patient, the patient, patient bed and related materials and the air kernel between the bed and detector can all contribute to the so called 'beam hardening' which sees this peak of the photon spectra shifting to a higher energy. So, even though the physical density and Z of the lanthanides are much lower than Pt or other elements with Z of 72–79, lanthanides can absorb X-rays significantly during common medical X-ray imaging and can be as radiopaque.

This dynamic nature of the linear attenuation coefficient is captured in the term cumulative linear coefficient (cumulative μ), which sums the products of multiplication of the X-ray imaging photon spectra (taken as a probability distribution) with the photon energy-dependent μ over the entire energy range of the photon spectra. Tofail et al. have compared the cumulative μ of NiTi, 316 stainless steel and Platinum-Enhanced Radiopaque Stainless Steel (PERSS®) with NiTi containing 5 and 7.5 atomic percent (at.%) erbium (Er), one of the RE lanthanides [1]. The improvement in radiopacity with the addition of Er is clear. This expectation is experimentally verified in NiTi–7.5 at.% RE prepared using conventional vacuum induction melting for alloying NiTi with gadolinium (Gd) and Er, which offered comparable visibility to that which has been achieved by adding 7.5 at.% Pt to NiTi.

The lack of radiopacity in NiTi alloys has been known for some time [19]. Improving radiopacity, while greatly important, requires more than a minor addition of a radiopaque element. Improvement of radiopacity by a few percent may require steps that can make a huge difference in terms of deployment, tracking, performance and retrieval. The analogy will be the growth of a country's gross domestic product (GDP) for which a single digit increase is considered significant. Current solutions aim for a partial enhancement using core wire, filled tubes, bands or markers of heavier and/or expensive elements such as Pt, tantalum (Ta) and gold (Au). Despite these measures, additional steps may be required to aide visibility during deployment for example using core wire and Pt dot markers on the same device [6]. The NiTi–7.5at% Pt ($\sim$22 wt% Pt in NiTi) is so expensive that they came onto the market as radiopaque markers only. There are other problems too. In many cases, the use of a dissimilar or noble

metal with NiTi may give rise to galvanic corrosion [6]. Radiopaque coating of NiTi devices with a film thickness greater than a 10 μm may also adversely affect SME and SE properties [20].

Experimental

Radiopacity Simulation

Data for various binary and ternary compositions were obtained using the XMuDat Program [21]. The programme converted mass attenuation coefficient data for elements, which was obtained from the work by Boone et al. [22], into those for compounds, composites and common materials. The mass attenuation coefficients were then converted into linear attenuation coefficients μ by multiplying with the density of the respective binary or ternary compositions. During simulation, RE elements were considered to be substituted for Ti in an equiatomic NiTi, while Pt would substitute for Ni. Imaging X-ray photon spectra were taken from experimentally obtained spectra reported in [22] for standard medical X-ray instruments operating at tube voltages between 40 and 120 kVp. These spectra have been normalised to act as a probability distribution of finding a photon at a given photon energy. Attenuation of the spectra was obtained by employing various filtration conditions including, where applicable, a simulated filtration condition of the Gastrointestinal (GI) region using the dimensions and chemistry (PMMA and Al plate) of a GI phantom (see below).

X-ray Fluoroscopy

Fluoroscopic X-ray images were taken by a Picker Clinix 1730F available at the Department of Radiology, University Hospital, Limerick, Ireland and a Ziehm Vision R available at the Department of Biomedical Engineering, Galway-Mayo Institute of Technology, Ireland. Standard setting of patient bed and, where applicable, a Nuclear Associates Model 07-649 CRDH Gastrointestinal (GI) Phantom was used. The Phantom was produced by Fluke Biomedical based on the Nationwide Evaluation of X-ray Trends (NEXT) survey by the FDA. Fluoroscopic images were then processed for Black & White contrast values, which were used to quantify the extent of radiographic contrast enhancement by normalising to the contrast of the binary NiTi of the equivalent form.

Powder Metallurgy

Commercially available binary NiTi ($A_f \cong -50$ °C) was atomised through a commercial vacuum induction melting gas atomization (IMGA) system. ErFe powders were atomised through a commercial electrode gas atomization (EIGA) system. Er–Ni powders of varying stoichiometry were purchased from American Elements. Ball milling was used to obtain a homogeneous powder mixture by quickly mixing the powders for 20 min in the presence of silicon nitride balls to enhance the mixing effect.

Sintering

Spark plasma sintering was carried out using a Dr. Sinterlab SPS 515S apparatus (Sumitomo Coal Mining Co. Ltd., Japan). Sintering was performed in vacuum ($\sim 10^{-3}$ Torr) and within a graphite die/punch assembly. A pulsed direct current was applied through the sample electrodes and through the sample with a characteristic time of a single pulse of about 3.3 ms. Uniaxial sintering pressure of 100 MPa was used along with a ramp rate of $\leq$25 °C and sintering temperature of 760 °C.

Hot Rolling

Hot rolling of the discs took place in a custom made motor-driven 12 groove square rolling rig. The material was heated to rolling temperature of 760 °C for 4 min between each pass. Area reductions per pass were limited to 6 %.

Cold Working and Training

Hot-rolled wires with diameter of $\sim$3.1 mm were cold drawn to 0.8 mm diameter wires using <4 % cross-section reductions. Intermediate air annealing at 600 °C for 10 min was undertaken between each drawing step. Final wire specimens were prepared for DSC and mechanical characterizations in both as drawn condition (4 % deformed) and after a annealing (at 400 °C for 20 min and at 530 °C for 5 min). Loading/unloading cycles were imposed on the samples wire for training of superelastic properties at 37 °C.

Differential Scanning Calorimetry

DSC measurements were carried out using a differential scanning calorimeter, Seiko model 520C, equipped with liquid nitrogen cooling system and calibrated with standard indium reference. During the DSC measurements, the temperatures associated to the second thermal cycle were taken into the range [−100; 100 °C] using 10 °C/min heating/cooling rate and the weight of the samples was about 30 mg.

Tensile Testing

Mechanical properties and recoverable strain were measured in tensile mode. Testing were performed with a MTS

2/M universal testing machine, equipped with pneumatic gripping and 25 mm gauge length extensometer, allowing for accurate deformation measurements. An MTS–Adamel-Liomargy environment chamber allowed for non-ambient temperature testing. Extended soaking at the desired temperature was performed to get uniform temperature conditions. Loading and unloading were performed under constant cross speed, settled to obtain an average strain rate lower than 10^{-4} m/m/s. The sample's diameter was 0.8 mm and a length of about 80 mm.

Results and Discussion

In Fig. 1a, we make a quick comparison of the X-ray fluoroscopy contrast of binary NiTi plates of 0.5 mm thickness (i) and 0.75 mm thickness (ii) with that of ternary radiopaque compositions including Pt, Pd and Er (Fig. 1a) along with some minor additions of Pd and Cr in comp 8 (NiTi3Er2Pd), comp9 (NiTi3Er2Pd0.25Cr), comp10 (NiTi2.25Er2Pd) and comp11 (NiTi2.25Er2Pd0.25Cr). Figure 1b and c shows a quantitative comparison of the radiopacity of NiTi–Pt and NiTi–Er with respect to that of the binary NiTi of the same thickness. We also include a simulated radiopacity contrast of 7.5 at.% tungsten-doped NiTi. Figure 1b and c shows that radiopacity improvement is a relative matter. The actual improvement in radiopacity will depend on the anatomical site in question, X-ray operation condition and filtration along with the device thickness and composition. In an atom for atom comparison (see 7.3 at.% Er and 7.6 at.% Pt, for example), the radiopacity of Er-alloyed NiTi is 5–10 % better than Pt-alloyed NiTi within the range of interest for medical X-ray (except for mammography, which is done at a much lower voltage, typically 17 kVp).

This is remarkable when one considers, fundamentally, that Er is lighter than Pt. So, the Beer–Lambert Law, which scales exponentially with a material's density and thickness, would have predicted that a denser material such as Pt (density 21.45 g/cc) would be absorb more and be more radiopaque than Er (density 9.07 g/cc). This is clearly not the case. We also added a calculated radiopacity for equivalent atomic addition NiTi7.5 at.% W under similar conditions. The radiopacity improvement is comparable to 7.3 at.% Er. This is again remarkable because tungsten is denser (19.3 g/cc). For a comparison based on equivalent weight (i.e. a gram of Er for a gram of Pt or W), Er will fare much better despite its lighter weight. Lighter weight of the Er alloys will have an additional advantage that the torque transduction through these wires will not need any change in the current manipulation device design. This is because the density of Er-alloyed NiTi ($\sim$7.5 g/cc for 7.5 at.% Er) is closer to binary NiTi (6.9 g/cc) than that with Platinum ($\sim$10.3 g/cc) or Tungsten (9.7 g/cc).

The addition of a ternary element into an otherwise binary equiatomic NiTi alloy is usually confronted with a few problems, e.g. deterioration in superelastic or shape memory properties, decrease in workability and increased cost of production and processing. Despite these challenges, ternary additions to binary NiTi have been attempted, very recently with the objective of increasing its X-ray visibility. Among the radiopaque elements, so far only the addition of Pt has been investigated in some useful form, e.g. wire and hypotube, but without describing any details on the materials processing or any quantitative value of the improvement in radiopacity [1, 4, 5]. Mehrabi et al. [23] reported a high hardness of W-alloyed NiTi. A near exponential increase in the hardness takes place as the W addition in NiTi increases up to 6 wt% W. Typical workable hardness ranges for NiTi alloys vary between 250 and 500 VHN. Higher amount of effort is needed when the hardness exceeds 400 VHN (e.g. in the case of alloying with Pt) [24].

Processing NiTi–Er alloys using conventional routes of vacuum melting, heat treatment and thermo-mechanical treatments poses a significant barrier due to the lack of hot and cold ductility of NiTi-RE systems. This topic has been described in our previous published work [10, 25]. We overcome these process barriers by resorting to a state-of-the-art spark plasma sintering method to produce near to theoretical density billets. In Ref. [10] we have demonstrated that billets produced in this method can be processed using conventional thermo-mechanical and mechanical processing towards the production of a number of useful forms including a wire. We use Er as a case study for the feasibility of processing radiopaque NiTi with RE elements to useful forms.

Powder metallurgy routes involve solid-state diffusion and localised melting. Er can be added in the form of powders of more stable intermetallic compounds of Er and Ni such as ErNi or Er_3Ni_2 (non-reactive route) to a pre-alloyed binary NiTi matrix. We have found that the alloys sintered using this route are generally ductile and much more workable than ingots made through the conventional vacuum melting route. The ductility and formability, however, go down when the amount of Ni increases in the Er–Ni compounds. Flat dicks, small cylinders and long billets could be produced in this way with density as high as 98 % of the theoretical density. Flat discs had been sintered using pre-alloyed ErNi with the equivalent amount of Er in the NiTi–Er varying between 4.5 and 12.5 at.%. These discs could then be cold worked to a thickness of 0.35 mm. By adding more ErNi to NiTi, a higher radiopacity could still be achieved.

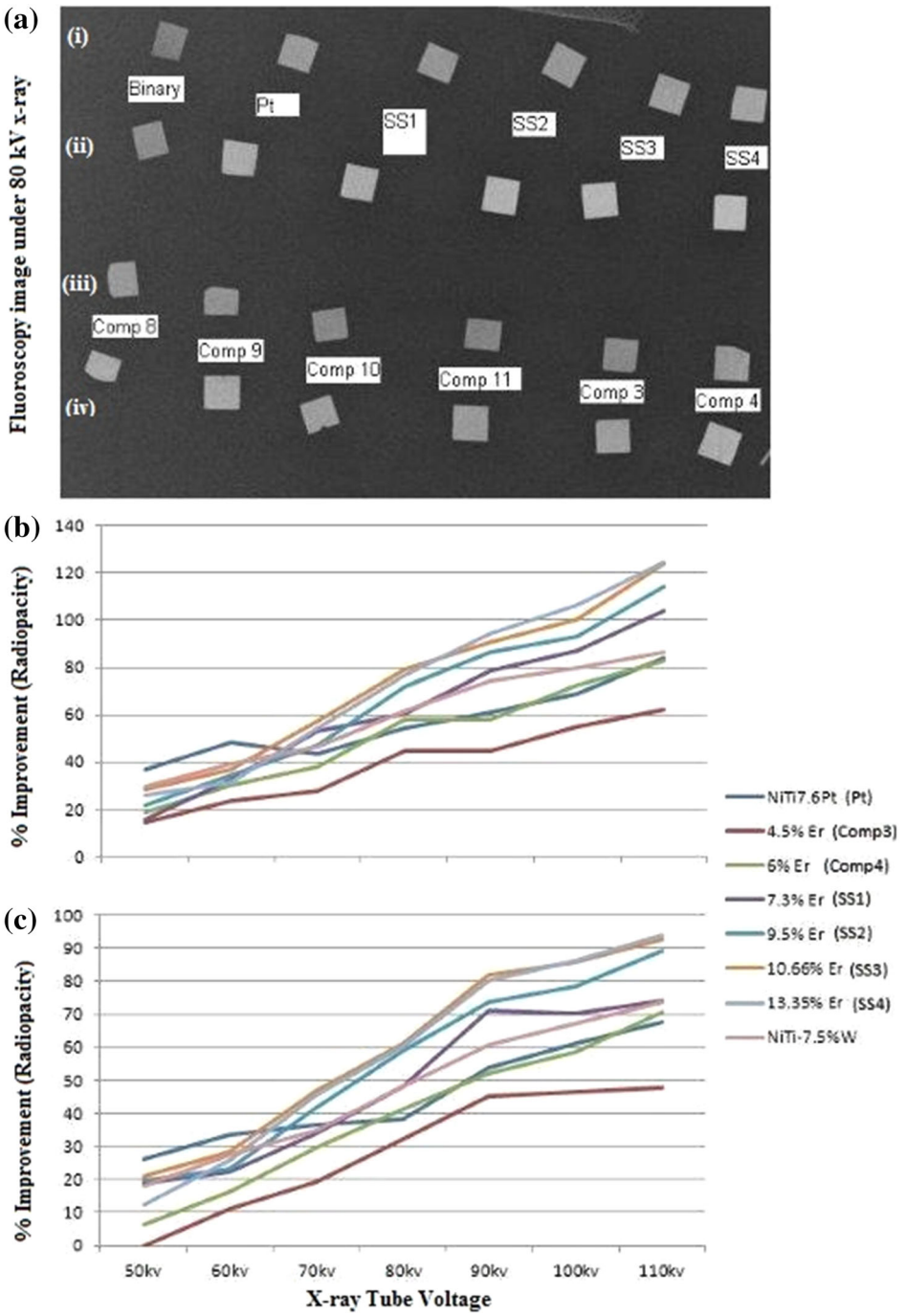

Fig. 1 **a** Static fluoroscopic X-ray images of binary, ternary, quaternary and pentanary NiTi alloys with various radiopaque elements Pt, Er and Pd with minor additions of Cr: Binary (NiTi), Pt (NiTi 7.6Pt), SS1 (NiTi7.3Er), SS2 (NiTi9.5Er), SS3 (NiTi10.66Er), SS4(NiTi13.35Er), comp3 (NiTi4.5Er), comp4 (NiTi6Er), comp 8 (NiTi3Er2Pd) comp9 (NiTi3Er2Pd0.25Cr), comp10 (NiTi2.25Er2Pd) comp11 (NiTi2.25Er2Pd0.25Cr). All elemental compositions are in atomic percentage. Plates in *rows* (*i*) and (*iii*) are about 500-micron thick. Plates in *rows* (*ii*) and (*iv*) are about 750-micron thick. **b** Quantitative improvements in radiopacity of Pt- and Er-alloyed NiTi plates (*rows* (*i*) and (*iii*)) of 500-micron thickness as a function of tube voltage normalised to the radiopacity of a 500-micron NiTi plate. Simulated improvement of radiopacity in NiTi–7.5W plate of the same thickness has also been included (**c**) Quantitative improvements in radiopacity of Pt- and Er-alloyed NiTi plates of 750-micron thickness (*rows* (*ii*) and (*iv*)) normalised to the radiopacity of a plate of binary NiTi plate of the same thickness. Simulated improvement of radiopacity in NiTi–7.5W plates of the same thickness has also been included (Color figure online)

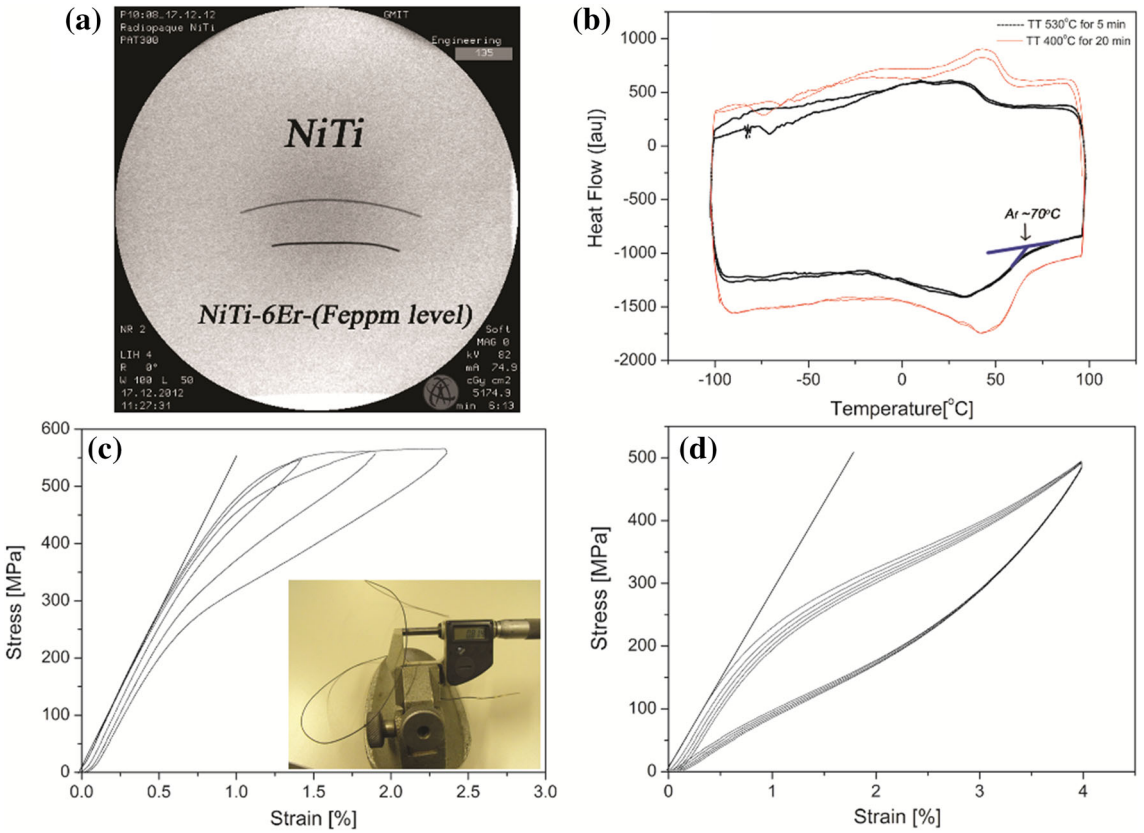

Fig. 2 **a** X-ray Fluoroscopic images of a binary and a NiTi–6 at.% Er wire showing ~80 % (±15 %) improvement in radiopacity at 80 kVp tube voltage with a GI phantom. **b** DSC curves of cold drawn NiTi–6 at.% Er wire after annealing at 400 °C for 20 min and 530 °C for 5 min. **c** Tensile test conducted at 70 °C on the 0.8 mm cold drawn wire (*inset figure*) after annealing. **d** Tensile test conducted at ~37 °C on the cold drawn 0.8 mm wire after loading/unloading training

The addition of metallic Er to NiTi was avoided as this causes excessive depletion of Ni from the matrix and results in the formation of brittle Ni-rich Ni–Er phases. The depletion of Ni from the NiTi matrix shifted the martensitic transformations to a higher temperature. A slightly Ni-rich composition of the NiTi starting powder (with austenite finish temperature, A_f ~−50 °C) could be used as a starting powder to compensate for the Ni-depletion. Further compensation could be achieved by introducing into the near-stoichiometric NiTi matrix $Ni_{51}Ti_{49}$ at.% (56 wt% Ni) and $Ni_{55}Ti_{45}$ at.% (60 wt% Ni). $Ni_{55}Ti_{45}$ at.% (Ni_{60}Ti wt%) is generally very hard to work so the amount that could be added required careful experimental design that balanced the overcompensation for depleted Ni with the final workability. We found that a 50/50 ratio between $Ni_{51}Ti_{49}$ at.% (Ni_{56}Ti wt%) and $Ni_{55}Ti_{45}$ at.% (Ni_{60}Ti wt%) retained enough ductility with a lowering of A_f by overcompensating for the depleted Ni.

The ductility of this alloy was remarkable, but, due to the localised depletion of Ni from NiTi matrix that forms Ni–Er phases, the austenitic transformation temperature, A_f rose to ~110 °C. A relatively weak secondary austenitic transformation peak had been observed to appear at lower temperatures (~15–30 °C). In this condition, the NiTi alloy is generally martensitic at the human body temperature. The alloy can still find medical application, since it is pseudoelastic and possesses approximately one half of the recoverable strain that has been available to an alloy that is austenitic or superelastic in the human body.

For biomedical applications, where superelasticity (SE) is required at body temperature, the A_f needs to be lowered to below the body temperature. The easiest route for this is to resort to a 'non-reactive' route, i.e. to use pre-alloyed Er–Ni powders that would not deplete the matrix from Ni. The workability decreases as the proportion of Ni in Er_xNi_y increases, while Er-rich compositions show a higher tendency of reacting to the Ni in the matrix. Overall, we found that the equiatomic composition ErNi to worked as the best choice as it provided at balanced reactivity with workability for this route. The A_f temperature of the sintered alloy was 5 °C which was lowered to −1 °C when rolled to 0.9 mm thickness, thus possessing both SME and body temperature SE.

Small cylindrical billets of 35 mm in diameter sintered in this way had been hot-rolled to a 3-mm diameter coarse wire to allow subsequent cold wire drawing to 0.8-mm

diameter. This wire, which contained 6 at.% Er, showed 80 ± 15 % improvement in radiopacity relative to a binary NiTi wire which was drawn to a 0.8 mm diameter (Fig. 2a). The cold drawn NiTi–6 at.% Er wire, after stress annealing at 400 °C for 20 min and 530 °C for 5 min, shows characteristic transformation temperatures as reported in DSC scans of Fig. 2b. Annealing lowered the martensitic transformation but A_f remained unchanged at ~70 °C. It also showed SE when tested at 70 °C (Fig. 2c). Ductility with 2.5 % recoverable strain and characteristic loading plateau is shown in Fig. 2c, but the A_f was still much higher than what is required to allow any SE at body temperature.

It is a common practice to 'train' cold worked binary NiTi to obtain an optimal balance between the residual stress and dislocations [20, 26]. By training, it is also possible to reduce the transformation temperatures. After 5–10 loading/unloading cycles at 37 °C, the cold worked alloy showed recoverable strain and SE (Fig. 2d). After cycling, up to deformation strain of 4 %, the wire showed a stable superelasticity with negligible residual permanent deformation after 50 loading/unloading cycles at body temperature. A combination of further training cycles and a tuning of the starting billet chemistry could be utilised in order to tune the A_f temperature further down to suit specific medical device and other low temperature SME and SE applications.

Conclusions

In summary, we demonstrate a 0.8-mm wire that was processed by hot rolling and cold wire drawing from a NiTi–6 at.% Er billet prepared by SPS. The wire exhibits SE at body temperature after training (~4 % recoverable strain) and enhances the radiopacity of binary NiTi by 80 ± 15 % at 80 kV X-ray tube voltage under a simulated gastrointestinal deployment. Higher visibility of these devices will provide ease of placement and manipulation of these devices, reduce patients' trauma during deployment and will significantly reduce radiation dose received by a patient in their lifetime.

Although we have focused on mainly Er addition, additions of other radiopaque RE elements can be accomplished in a similar manner. Also, a higher amount of radiopaque element Er can be added without compromising much on the desirable SME and SE properties and workability. These processes are fully scalable to large volume productions. The presented work thus opens the door for practical implementation of relatively cheaper, functional radiopaque NiTi-RE for minimally invasive surgery. Due to the tunability of SME and SE of NiTi-RE, there may arise a number of novel non-biomedical applications, e.g. in high temperature actuation and transduction.

Acknowledgments This project has been funded under the Innovation Partnership Programme of the Enterprise Ireland (Grant nos.: IP 2005-292; IP 2008-545 and IP 2011-0111). Authors acknowledge Professor Tim McGloughlin, Department of Mechanical, Aeronautical and Biomedical Engineering, University of Limerick for his advice on radiopacity measurements.

The Field Emission SEM was funded by the Higher Education Authority (HEA) under the PRTLI 4 program within the INSPIRE consortium. Dr. SinterLab Spark Plasma Sintering machine was funded by the HEA under the Laboratory Refurbishment Grant 2008. Thanks also to M.Pini and N.Bennato of CNR IENI Lecco for their technical assistance in material processing.

References

1. Lin B, Gall K, Maier HJ, Waldron R (2009) Structure and thermomechanical behavior of NiTiPt shape memory alloy wires. Acta Biomater 5:257
2. Stoel BC (1996) PhD Thesis, Leiden University, Leiden
3. Carr S (2011) PhD Thesis, University of Limerick, Limerick
4. Lin Z, Hsiao H-M, Mackiewicz D, Anukhin B, Pike K (2009) Anisotropic behavior of radiopaque NiTiPt hypotube for biomedical applications. Adv Eng Mater 11:B189–B193
5. Boylan JF (2004) SMST 2003. In: Pelton AR, Duerig TW (eds) Proceedings of international conference on shape memory and superelasitc technologies 2003, Pacific Gove, California, pp 1–4, 2004
6. Stöckel D, Pelton A, Duerig T (2004) Self-expanding nitinol stents: material and design considerations. Eur Radiol 14:292
7. Craig CH, Radisch HR, Trozera TA, Turner PC, Govier RD, Vesely EJ, Gokcen NA, Friend CM, Edwards MR (2003) Special technical publications: stainless steels for medical and surgical applications, ASTM International, STP-11151S
8. Tofail SAM, Carlson J, Gandhi AA, ButlerJ, Tiernan P, O'Donoghue L (2013) United States Patent, 8440031
9. Tofail SAM, Carlson J, Carr S, Devereux P, Haverty D, Lavelle SJ, McGloughlin T (2015) Nickel-titanium alloy including a rare earth element. US Patent 9,103,006
10. Tofail SAM, Butler J, Gandhi AA, Carlson JM, Lavelle S, Carr S, Tiernan P, Warren G, Kennedy K, Biffi CA, Bassani P, Tuissi A (2014) X-ray visibility and metallurgical features of NiTi shape memory alloy with erbium. Mater Lett 137:450–454
11. Goldstein W, Buehler J, Wiley RC (1965) Naval Ordnance Laboratory Report NOLTR, 64-235
12. Zhao X, Wang W, Chen L, Liu F, Chen G, Huang J, Zhang H (2008) Two-stage superelasticity of a Ce-added laser-welded TiNi alloy. Mater Lett 62:3539–3541
13. Zhao X, Wang W, Chen L, Liu F, Huang J, Zhang H (2008) Microstructures of cerium added laser weld of a TiNi alloy. Mater Lett 62:1551–1553
14. Jingqi L, Shunkang P, Yinghong Z (2002) The isothermal section of the phase diagram of the Dy–Mn–Ti ternary system at 773 K. J Alloys Compd 313:93
15. Jingqi L, Ke G (2000) The isothermal section of the phase diagram of the La–Ni–Ti ternary system at 673 K. J Alloys Compd 312:121–123
16. Jingqi L, Yinghong Z, Yeqi H (2004) The 773 K isothermal section of the ternary phase diagram of the Nd–Ni–Ti. J Alloy Compd 368:180–181

17. Hasegawa B (1987) The physics of medical X-ray imaging. Medical Physics Publishing Corporation, Madison
18. Aichinger H, Dierker J, Joite-Barfuß S, Säbel M (2004) Radiation exposure and image quality in X-ray diagnostic radiology: physical principle and clinical application. Springer, Berlin
19. Rabkin DJ, Lang EV, Brophy DP (2000) Nitinol properties affecting uses in interventional radiology. J Vasc Interv Radiol 11:343–350
20. Otsuka K, Wayman CM (1998) Shape memory materials. Cambridge University Press, Cambridge
21. Nowotny R (1998) XMuDat: photon attenuation data on PC, Version 1.0.1. International Atomic Energy Agency: Nuclear Data Service report, IAEA-NDS-195
22. Boone JM, Chavez AE (1996) Comparison of X-ray cross sections for diagnostic and therapeutic medical physics. Med Phys 23(12):1997–2005
23. Mehrabi K, Bahmanpourb H, Shokuhfar A, Kneissl A (2008) Influence of chemical composition and manufacturing conditions on properties of NiTi shape memory alloys. Mater Sci Eng, A 481–482:693–696
24. Boylan J (2014) The development of radiopaque NiTiNol, SMST-2003. In: Pelton AR, Duerig T (eds) Proceedings of the international conference on shape memory and superelasitc technologies, pp 1–6, 2014
25. Tofail SAM, Gandhi AA, Butler J, O'Donoghue L, McNamara K, Tiernan P, McGloughlin T, Carlson JC, Lavelle S, Biffi CA, Tuissi A (2014) Workability of Radiopaque Er-NiTi, SMST-2013. In: The international conference on shape memory and superelastic technologies (SMST), ASM International, pp 189–190, 2014
26. Tuissi A, Bassani P, Mangioni A, Toia L, Butera F (2006) Fabrication process and characterization of NiTi Wires for Actuators. In: Mertnamm M (ed) Proceedings of the international conference on shape memory and superelastic technologies SMST 2004, ASM Int, pp 501–508, 2006